Measuring Light Yukawa couplings and Flavour Changing Neutral Currents in Higgs hadronic decays at the FCC-ee

Michele Selvaggi[1*]

[1]CERN, Geneva, Switzerland.

Corresponding author(s). E-mail(s): michele.selvaggi@cern.ch;

Abstract

We present a study of the sensitivity of the FCC-ee to Higgs decays involving light quarks (up and down) and flavor-changing neutral currents (FCNCs). Using a dedicated multivariate analysis, we exploit the $\mathbf{e^+e^- \rightarrow \nu\bar{\nu}H(jj)}$ final state to identify, classify, and extract hadronic Higgs decays. We derive 95% CL upper limits on $\mathbf{H \rightarrow uu}$, **dd**, **bs**, **bd**, **sd**, and **cu**, improving upon existing bounds by up to an order of magnitude. These results highlight the unique potential of the FCC-ee to probe the light Yukawa sector and test for extensions of the Standard Model that induce FCNCs in the Higgs sector.

1 Introduction

The discovery of the Higgs boson has opened the door to direct tests of the Higgs–fermion Yukawa interactions across all three generations. In the Standard Model (SM), the Yukawa coupling $\mathrm{y_f}$ is proportional to the fermion mass ($\mathrm{y_f} \sim \mathrm{m_f/v}$ with $v \simeq 246$ GeV). First generation quarks have extremely small Yukawa couplings therefore measuring H couplings to up and down quarks is experimentally challenging. It is however required to confirm that the Higgs mechanism generates mass even for the lightest quarks and to probe potential new physics that could modify the Yukawa structure. Direct searches for Higgs decays to light quarks at the LHC face very large QCD backgrounds. The $\mathrm{H \to u\bar{u}}$ and $\mathrm{H \to d\bar{d}}$ modes are too rare to be measured at the LHC, and even the $\mathrm{H \to s\bar{s}}$ (strange quark) decay is difficult to isolate experimentally because of the absence of dedicated hadron identification in LHC experiments. The existing bounds are derived from searches for rare exclusive decays and global coupling fits. No significant deviation from $\kappa_{\mathrm{u,d}} \equiv \mathrm{y_{u,d}/y^{SM}_{u,d}} = 1$ is currently observed, and the most constraining projections at the HL-LHC [1] on light Yukawas give $|\kappa_{\mathrm{u}}| < 500$ and $|\kappa_{\mathrm{d}}| < 250$.

In the SM, off-diagonal Yukawa couplings are zero, which ensures the absence of tree-level flavor-changing neutral currents (FCNCs) mediated by the Higgs boson. At higher orders, the SM induces tiny effective FCNC couplings (via loops), but such effects are far below observable levels due to the GIM mechanism and the smallness of the light-quark masses. Higgs-mediated FCNCs can arise in extensions of the Higgs sector such as Two Higgs Doublet Models (2HDM) or the MSSM. Any hint of Higgs-mediated FCNC, would be a clear signal of new physics. Experimental constraints on possible Higgs FCNC couplings are dominated by precision measurements in the flavor sector. In the down-quark sector, the best bounds come from neutral meson mixing B_s^0–$\bar{B}_s^0$ and B_d^0–$\bar{B}_d^0$ mixing, constraining potential Hbs and Hbd couplings. Likewise, the neutral K^0–$\bar{K}^0$ system can help constrain Hsd transitions and, in the up-quark sector, D^0–$\bar{D}^0$ mixing constrain respectively the Hsd and Hcu couplings. No significant FCNC involving the Higgs has been observed in any quark sector. Although direct searches for $H \to bs$ or $H \to cu$ are hardly feasible at the LHC, the stringent indirect limits from K, B, and D physics, together with global fits, loosely constrain the possibility of off-diagonal Higgs couplings. The SM values of Higgs decays to light Yukawas (uu and dd)and bs, bd, cu, and sd are given in Table 1, along with the current upper limits on their branching ratios and effective couplings, where available.

decay channel	SM Branching Ratio ($\mathcal{B}$)	upper limit $\mathcal{B}$	upper limit $\|\kappa_i\|$
$\mathrm{H \to uu}$	1.2×10^{-7}	3×10^{-2}	500
$\mathrm{H \to dd}$	5.5×10^{-7}	7×10^{-3}	250
$\mathrm{H \to bs}$	8.9×10^{-8}	2×10^{-3}	
$\mathrm{H \to bd}$	3.8×10^{-9}	10^{-3}	
$\mathrm{H \to cu}$	2.7×10^{-20}	2×10^{-2}	
$\mathrm{H \to sd}$	1.9×10^{-15}	-	-

Table 1 Standard Model Branching ratios for various Higgs hadronic decay channels and existing bounds.

In this note, we discuss the expected sensitivity to hadronic light Yukawa couplings of the Higgs boson and its flavor off-diagonal decays at the FCC-ee. A phenomenological investigation of such a possibility has been documented in Ref. [2]. Here, by using state-of-art FCC-ee detector simulation, analysis techniques, flavor tagging tools, we demonstrate that the FCC-ee can surpass current bounds on all these rare decay channels. This improvement is made possible by the exceptionally low levels of QCD background, the use of high-precision detectors with excellent impact parameter resolution and particle identification, as well as recent advances in powerful jet flavor tagging techniques that exploit the full jet content [3, 4].

2 Event Samples

Monte Carlo events are simulated using the IDEA detector [5] concept and the fast simulation framework Delphes [6–8]. The reconstruction algorithm is based on a particle-flow algorithm. The generated data is part of the winter 2023 production campaign [9].

The list of samples is summarized in Table 2. The samples are generated with the Whizard [10, 11] event generator, using the Pythia6 [12] parton shower and hadronization model. The cross sections are calculated at leading order (LO) using the Whizard generator. The samples are generated at a center-of-mass energy of 240 GeV. The samples include both signal and background processes.

Process	Sample name	Cross section (pb)
$e^+e^- \to \nu\nu H \to \nu\nu bb$	`wzp6_ee_nunuH_Hbb_ecm240`	0.03
$e^+e^- \to \nu\nu H \to \nu\nu cc$	`wzp6_ee_nunuH_Hcc_ecm240`	1.34×10^{-3}
$e^+e^- \to \nu\nu H \to \nu\nu ss$	`wzp6_ee_nunuH_Hss_ecm240`	1.11×10^{-5}
$e^+e^- \to \nu\nu H \to \nu\nu dd$	`wzp6_ee_nunuH_Hdd_ecm240`	9.70×10^{-9}
$e^+e^- \to \nu\nu H \to \nu\nu uu$	`wzp6_ee_nunuH_Huu_ecm240`	4.16×10^{-9}
$e^+e^- \to \nu\nu H \to \nu\nu bs$	`wzp6_ee_nunuH_Hbs_ecm240`	8.90×10^{-8}
$e^+e^- \to \nu\nu H \to \nu\nu bd$	`wzp6_ee_nunuH_Hbd_ecm240`	3.80×10^{-9}
$e^+e^- \to \nu\nu H \to \nu\nu sd$	`wzp6_ee_nunuH_Hsd_ecm240`	1.20×10^{-8}
$e^+e^- \to \nu\nu H \to \nu\nu cu$	`wzp6_ee_nunuH_Hcu_ecm240`	2.70×10^{-20}
$e^+e^- \to \nu\nu H \to \nu\nu gg$	`wzp6_ee_nunuH_Hgg_ecm240`	3.78×10^{-3}
$e^+e^- \to \nu\nu H \to \nu\nu\tau\tau$	`wzp6_ee_nunuH_Htautau_ecm240`	2.90×10^{-3}
$e^+e^- \to \nu\nu H \to \nu\nu WW$	`wzp6_ee_nunuH_HWW_ecm240`	9.94×10^{-3}
$e^+e^- \to \nu\nu H \to \nu\nu ZZ$	`wzp6_ee_nunuH_HZZ_ecm240`	1.22×10^{-3}
$e^+e^- \to qqH$	`wzp6_ee_qqH_ecm240`	0.14
$e^+e^- \to WW$	`p8_ee_WW_ecm240`	16.44
$e^+e^- \to ZZ$	`p8_ee_ZZ_ecm240`	1.36
$e^+e^- \to qq$	`p8_ee_Zqq_ecm240`	52.65

3 Analysis Strategy

3.1 Event pre-selection

Among all the possible ee $\to$ ZH final state, the most favorable is the Z($\nu\nu$) channel. The Z boson decays into two neutrinos, which are not detected, while the Higgs boson

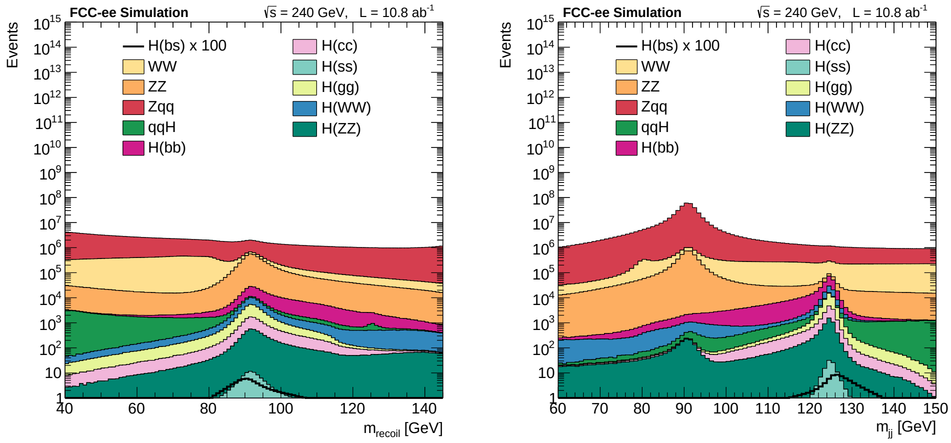

Fig. 1 Left: Recoil mass (m_{recoil}) distribution at preselection level, showing a peak around the Z boson mass for signal events with $\mathrm{Z} \to \nu\bar{\nu}$. Right: Dijet invariant mass (m_{jj}) distribution at preselection level, illustrating the contribution from various hadronic Higgs decays. Both distributions include signal and background processes before event categorization.

decays into a pair of light quarks. The final state consists of two jets from the Higgs decay and missing momentum from the Z decay. The analysis strategy is similar to the one used in the analysis of the Higgs boson decaying into bb,cc,ss,gg at the FCC-ee [13].

The main backgrounds can be categorized as both reducible and irreducible. The dominant reducible backgrounds include diboson processes such as $\mathrm{ZZ} \to \nu\nu\mathrm{qq}$ and $\mathrm{WW} \to \ell\nu\mathrm{qq}'$ where the charged lepton is not reconstructed, as well as Z+jets events where the $Z \to \nu\nu$ decay is accompanied by QCD jets that mimic the hadronic Higgs signature. These processes can fake the signal topology due to genuine missing transverse energy and hadronic activity. Irreducible backgrounds are primarily due to SM Higgs boson production where the Higgs decays hadronically: $\mathrm{H} \to \mathrm{b\bar{b}}, \mathrm{c\bar{c}}, \mathrm{s\bar{s}}, \mathrm{gg}$, or via hadronic decays of intermediate bosons such as $\mathrm{H} \to \mathrm{WW}^*$, $\mathrm{H} \to \mathrm{ZZ}^*$, and $\mathrm{H} \to \tau\tau$ with both τ-leptons decaying hadronically. These irreducible processes share the same final state signature as the signal.

Events are pre-selected by vetoing the presence of isolated high momentum ($p > 20$ GeV) leptons (electrons or muons). The presence of a lepton would indicate the presence of a Z boson decaying into a lepton pair, which will be extracted in an orthogonal analysis. The presence of a lepton also indicates the presence of a leptonically decayed W boson, which is a background. In addition, we compute the polar angle of the missing momentum with respect to the beam axis θ_{miss} and require $|\cos\theta_{\mathrm{miss}}| < 0.85$. This requirement reduces the background from the Z boson decaying into two quarks. The missing momentum vector $\mathbf{p_{miss}}$ is computed as minus the vector sum of the momentum of all the reconstructed particles in the event.

Jets are reconstructed using the Durham algorithm [14] in exclusive mode, i.e., by clustering all the particles in the events into two jets. A Graph Neural Network (GNN) jet flavour tagger [3, 4] is then used to assign each jet a probability of originating from

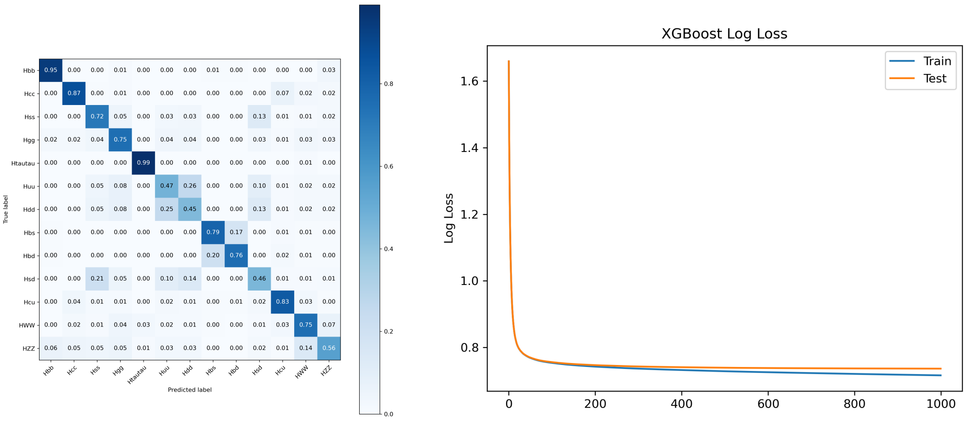

Fig. 2 Left: Confusion matrix of the BDT classifier, showing the fraction of events correctly classified into their respective classes (diagonal elements) and misclassifications (off-diagonal elements). Right: Logarithmic loss (cross-entropy) evaluated on test and training as a function of the training iterations.

one of seven species: gluon (g), up (u), down (d), strange (s), charm (c), bottom (b), or tau (τ). The tagger uses the information of all particle-flow candidates within a jet, including kinematic, impact parameters, and particle identification (cluster-counting and time-of-flight).

The recoil mass, $\mathrm{m_{recoil}}$, is computed using energy and momentum conservation with respect to the total visible system in the event. It is defined as the invariant mass of the system recoiling against the visible final-state particles, and for signal events, it peaks around the Z boson mass, corresponding to the $\mathrm{Z} \to \nu\nu$ missing mass. This variable is particularly effective in rejecting backgrounds such as $\mathrm{Zq\bar{q}}$, which lacks genuine missing momentum and thus populates low recoil mass regions. The dijet invariant mass $\mathrm{m_{jj}}$ is constructed from the four-momenta of the two jets, assumed to originate from the hadronic decay of the Higgs boson. In contrast, WW and ZZ processes, exhibit different correlations between $\mathrm{m_{jj}}$ and $\mathrm{m_{recoil}}$. Combining these two variables provides strong discriminating power against the non-resonant SM backgrounds. The corresponding distributions are shown in Figure 1. No selection is applied of these variables at this stage, since the extended spectrum is used to measure the background contributions from the side-bands (see discussion in Section 3.3).

3.2 Separation of Higgs hadronic decay modes

To discriminate signal events from the irreducible backgrounds from Higgs SM hadronic decays, a Boosted Decision Tree (BDT) classifier is trained using a set of kinematic variables and jet tagging scores. These input variables encode information about the properties of the reconstructed jets, the event topology, and flavor-tagging scores for different quark and gluon hypotheses. The BDT is trained in a multiclass configuration with 13 classes, each corresponding to a distinct Higgs decay channel, including both SM and potential flavor-changing final states.

The full list of classes includes $\mathrm{H} \to \mathrm{b\bar{b}}$, $\mathrm{H} \to \mathrm{c\bar{c}}$, $\mathrm{H} \to \mathrm{s\bar{s}}$, $\mathrm{H} \to \mathrm{d\bar{d}}$, $\mathrm{H} \to \mathrm{u\bar{u}}$, $\mathrm{H} \to \mathrm{b\bar{s}}$, $\mathrm{H} \to \mathrm{b\bar{d}}$, $\mathrm{H} \to \mathrm{s\bar{d}}$, $\mathrm{H} \to \mathrm{c\bar{u}}$, $\mathrm{H} \to \mathrm{gg}$, $\mathrm{H} \to \tau\tau$, $\mathrm{H} \to \mathrm{WW}$, and $\mathrm{H} \to \mathrm{ZZ}$. The

BDT uses the following input variables to exploit differences in event topology and flavor composition across all possible $\mathrm{H} \to \mathrm{jj}$ decay modes.

Jet tagging scores: The jet flavor tagging scores include variables such as $\mathrm{score_U}$, $\mathrm{score_D}$, $\mathrm{score_S}$, $\mathrm{score_C}$, $\mathrm{score_B}$, $\mathrm{score_\tau}$, and $\mathrm{score_G}$, computed separately for each of the two jets. These scores represent the likelihood that a jet originates from a specific particle type (up, down, strange, charm, bottom quark, tau lepton, or gluon), as determined by the flavor tagging algorithm. They are essential for distinguishing the Higgs to light quark modes and FCNCs from the other SM Higgs decays.

Jet substructure: variables such as $\mathrm{d_{12}}$, $\mathrm{d_{23}}$, $\mathrm{d_{34}}$, $\mathrm{d_{45}}$, and $\mathrm{d_{56}}$ describe the internal structure of jets during the clustering process. Each $\mathrm{d_{ij}}$ represents the distance measure at step $j \to i$ of the jet recombination sequence. These variables are particularly useful for separating $\mathrm{H} \to \mathrm{jj}$ events from $\mathrm{H} \to \mathrm{WW/ZZ} \to \mathrm{jjjj}$ events.

In Figure 4 (Left), we show the confusion matrix of the BDT classifier, which illustrates the classifier's performance in separating the different Higgs decay channels. The diagonal elements represent the fraction of events correctly classified into their respective classes, while the off-diagonal elements indicate misclassifications. The BDT classifier achieves a good separation between the different Higgs decay channels, with high purity for the signal classes. The exception is the separation between Huu and Hdd, which is notoriously difficult, given the similarity between these two decay modes. The logarithmic loss (cross-entropy) evaluated on test and training as a function of the training iterations is shown in Figure 4 (Right). The BDT classifier converges to a low value of the logarithmic loss, indicating good performance in separating the different Higgs decay channels.

3.3 Event categorisation and signal extraction

Event categorization: To extract the signal contribution for each hadronic Higgs decay mode $\mathrm{H} \to \mathrm{jj}$, we first categorise events based on the BDT output score. For each event, the BDT assigns a score $\mathrm{S(H \to X)}$ for each of the 13 Higgs decay hypotheses. An event is associated to a given Higgs decay channel, e.g. $\mathrm{H} \to \mathrm{b\bar{b}}$, if its corresponding score $\mathrm{S(H \to b\bar{b})}$ is the largest:

$$\mathrm{S(H \to b\bar{b})} > \max\left\{\mathrm{S(H \to X)}\right\}, \quad \mathrm{X} \in \{\mathrm{c\bar{c}, s\bar{s}, gg, u\bar{u}, d\bar{d}, b\bar{s}, b\bar{d}, s\bar{d}, c\bar{u}}, \tau\tau, \mathrm{WW, ZZ}\}.$$

This approach ensures that the selected region is as pure as possible for each decay hypothesis, creating a set of 13 mutually exclusive signal-enriched regions: Hbb-like, Hcc-like, Huu-like, Hbs-like, HWW-like, .. etc.

Each of these signal-like regions is further divided into three subcategories — low purity (LP), medium purity (MP), and high purity (HP) — based on the value of the BDT score for the corresponding decay. This yields a total of $13 \times 3 = 39$ exclusive event categories.

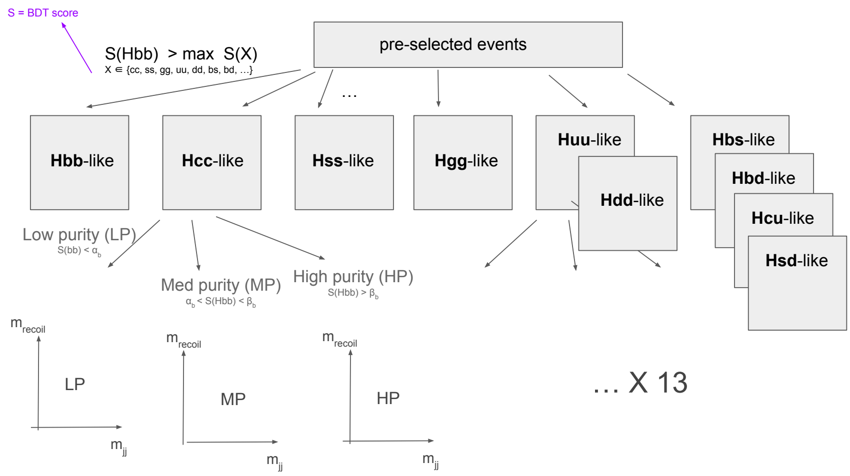

Fig. 3 Event categorization and signal extraction strategy

To illustrate the effectiveness of the BDT-based categorization, Figure 4 (left) shows the normalized distribution of the $H \to bs$ BDT score for signal and background Higgs decays. The signal events peak at large score values, allowing for the definition of a high-purity region dominated by $H \to bs$-like topologies. After selecting events in this high-purity category, the dijet invariant mass distribution (Figure 4, right) shows a clear enhancement of the signal over the background. In addition, the resonant contributions from other hadronic Higgs decays such as $H \to b\bar{b}$, $c\bar{c}$, and gg are substantially reduced.

Signal extraction: The variables m_{jj} and m_{recoil} are a key ingredient of the signal extraction strategy, since they provide complementary sensitivity to the Higgs boson and Z boson kinematics, respectively.

The signal strengths parameters of interests (POIs) for each of the 13 Higgs decay channels are then extracted simultaneously via a binned two-dimensional maximum likelihood fit to the distributions of m_{jj} and m_{recoil} in each of the 39 categories. This strategy, illustrated schematically in Fig. 3, enables the robust and simultaneous extraction of the light Yukawa and FCNC signal contributions, even in the presence of overlapping and more abundant SM Higgs hadronic decay signatures.

The $e^+e^- \to ZH$, ZZ, WW, and $Zq\bar{q}$ backgrounds considered in the fit are assigned a conservative normalization uncertainty of 10%. However, the fit is able to constrain these uncertainties effectively, reducing their post-fit impact uncertainty the level of 1% or less per background component, thanks to the high statistics and discriminating power in the sidebands of the two-dimensional mass distributions.

4 Results

The upper limits are extracted from a global simultaneous fit of 13 POIs across 39 event categories over the 2D m_{jj} and m_{recoil} distributions, as discussed in the previous

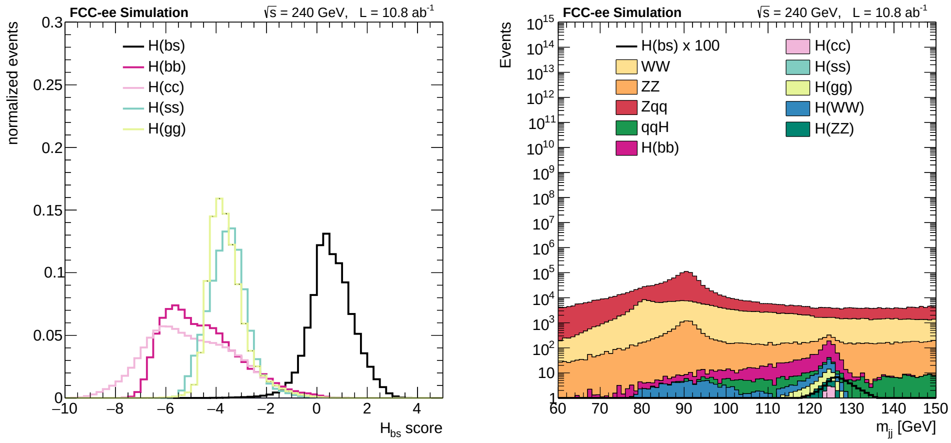

Fig. 4 Left: Normalized distribution of the BDT score for the $H \to bs$ decay hypothesis, compared to other Standard Model Higgs decays. The $H \to bs$ events cluster toward high values, enabling the definition of a high-purity selection region. Right: Dijet invariant mass (m_{jj}) distribution after applying a high-purity $H \to bs$ selection (corresponding to $H_{bs} > 0$). The contribution from dominant resonant Higgs decays (e.g. $H \to b\bar{b}, c\bar{c}, s\bar{s}, gg$) is significantly suppressed, demonstrating the discriminating power of the classifier.

section. The 95% confidence level (CL) upper limits are derived for each of the processes $H \to uu$, $H \to dd$, $H \to bs$, $H \to bd$, $H \to sd$, and $H \to cu$ using an integrated luminosity of 10.8 ab^{-1}. While the limits reported here are derived from a simplified treatment (using twice the 68% error bands as an estimate of 95% CL limits), they provide comparable results to previous phenomenological studies [2]. We stress that the same fit simultaneously extracts the contributions of the dominant SM hadronic Higgs decays: $H \to b\bar{b}$, $H \to c\bar{c}$, $H \to s\bar{s}$, and $H \to gg$. The extracted values for these channels are found to be in good agreement with the dedicated analysis reported in Ref. [13], which further validates the robustness of the method used in this work.

Table 2 Summary of 95% CL upper limits on the branching ratios of rare and FCNC Higgs decays, assuming 10.8 ab^{-1} using only the $\nu\nu H(jj)$ channel at $\sqrt{s} = 240$ GeV, compared to SM predictions and existing indirect constraints.

Decay	SM Prediction	this work (95% CL)	current constraints
$H \to uu$	1.2×10^{-7}	$< 1.2 \times 10^{-3}$	3×10^{-2}
$H \to dd$	5.5×10^{-7}	$< 1.2 \times 10^{-3}$	7×10^{-3}
$H \to bs$	9×10^{-8}	$< 3.1 \times 10^{-4}$	$< 1.6 \times 10^{-3}$
$H \to bd$	4×10^{-9}	$< 2.2 \times 10^{-4}$	$< 10^{-3}$
$H \to cu$	3×10^{-20}	$< 2.0 \times 10^{-4}$	$< 2 \times 10^{-3}$
$H \to sd$	2×10^{-15}	$< 6.5 \times 10^{-4}$	—

The analysis yields competitive constraints on all the considered Higgs decay channels. A summary of the obtained results is presented in Table 2, where the expected bounds are compared to the SM predictions and, where available, to indirect limits derived from low-energy observables (e.g. meson mixing).

5 Conclusions

The FCC-ee has the potential to significantly improve upon current indirect constraints both for light-quark Yukawa couplings and for hadronic flavor-changing Higgs decays. For these processes, the direct reach achieved in this analysis is better than the bounds derived from flavor observables. These improvements are made possible by the combination of advanced flavor-tagging techniques powered by machine learning and the exceptional performance of the FCC-ee detectors. In particular, the excellent particle identification and precise impact parameter resolution enable highly efficient and pure identification of bottom, charm, and strange jets, which is critical to the measurements presented in this work.

Acknowledgements

This work has been partly supported by the Future Circular Collider Innovation Study (FCCIS) project, that has received funding from the European Union's Horizon 2020 research and innovation programme under grant No 951754. I would like to thank Louis Portales for helping with the definition and production of the samples used in this analysis.

References

[1] J. de Blas, et al., Higgs Boson Studies at Future Particle Colliders. JHEP **01**, 139 (2020). https://doi.org/10.1007/JHEP01(2020)139. arXiv:1905.03764 [hep-ph]

[2] J.F. Kamenik, A. Korajac, M. Szewc, M. Tammaro, J. Zupan, Flavor-violating Higgs and Z boson decays at a future circular lepton collider. Phys. Rev. D **109**(1), L011301 (2024). https://doi.org/10.1103/PhysRevD.109.L011301. arXiv:2306.17520 [hep-ph]

[3] F. Bedeschi, L. Gouskos, M. Selvaggi, Jet flavour tagging for future colliders with fast simulation. Eur. Phys. J. C **82**(7), 646 (2022). https://doi.org/10.1140/epjc/s10052-022-10609-1. arXiv:2202.03285 [hep-ex]

[4] S. Aumiller, D. Garcia, M. Selvaggi. Jet Flavor Tagging Performance at FCC-ee (2024). https://doi.org/10.17181/8g834-jv464

[5] The IDEA detector concept for FCC-ee (2025). arXiv:2502.21223 [physics.ins-det]

[6] de Favereau, J. and Delaere, C. and Demin, P. and Giammanco, A. and Lemaître, V. and Mertens, A. and Selvaggi, M., DELPHES 3, A modular framework for fast simulation of a generic collider experiment. JHEP **02**, 057 (2014). https://doi.org/10.1007/JHEP02(2014)057. arXiv:1307.6346 [hep-ex]

[7] Various authors. FCC-ee IDEA detector DELPHES card. https://github.com/delphes/delphes/blob/master/cards/delphes_card_IDEA.tcl

[8] T. Madlener, V. Volkl, C. Helsens, M. Chrzaszcz, F. Gaede. key4hep/k4simdelphes: v00-02-01 (2022). https://doi.org/10.5281/zenodo.7256903

[9] FCC. Delphes fccee physics events winter2023 production (idea detector) (2025). URL https://fcc-physics-events.web.cern.ch/fcc-ee/delphes/winter2023/idea/. Accessed: March 2025

[10] W. Kilian, T. Ohl, J. Reuter, WHIZARD: Simulating Multi-Particle Processes at LHC and ILC. Eur. Phys. J. C **71**, 1742 (2011). https://doi.org/10.1140/epjc/s10052-011-1742-y. arXiv:0708.4233 [hep-ph]

[11] Jürgen Reuter at al. New developments on the whizard event generator (2023). https://doi.org/10.48550/arXiv.2307.14900

[12] T. Sjostrand, S. Mrenna, P.Z. Skands, PYTHIA 6.4 Physics and Manual. JHEP **05**, 026 (2006). https://doi.org/10.1088/1126-6708/2006/05/026. arXiv:hep-ph/0603175

[13] A. Del Vecchio, J. Eysermans, L. Gouskos, G. Iakovidis, A. Maloizel, G. Marchiori, M. Selvaggi. FCC note: Measurement of Higgs boson hadronic decays with $Z(\nu\bar{\nu}\,\ell\ell, jj)$ H events at FCC-ee at $\sqrt{s} = 240\,\text{GeV}$ (2023). https://doi.org/10.17181/9pr7y-3v657

[14] S. Catani, Y.L. Dokshitzer, M. Olsson, G. Turnock, B.R. Webber, New clustering algorithm for multi - jet cross-sections in e+ e- annihilation. Phys. Lett. B **269**, 432 (1991). https://doi.org/10.1016/0370-2693(91)90196-W